Available online at www.sciencedirect.com
SCIENCE DIRECT®
ELSEVIER
International Journal of Solids and Structures 42 (2005) 4077–4098
INTERNATIONAL JOURNAL OF SOLIDS and STRUCTURES
www.elsevier.com/locate/ijsolstr

Thermo-mechanical consequences of phase transformations in the heat-affected zone using a cyclic uniaxial test

Yannick Vincent [a], Jean-François Jullien [b,*], Philippe Gilles [c]

[a] *ESI – Group 84 Bd Vivier Merle 69485 Lyon Cedex, France*
[b] *Institut National de Sciences Appliquees INSA – Lyon, Laboratoire de Mecanique des Contacts et des Solides Batiment JCA Coulomb, 20 Avenue Albert Einstein, 69621 Villeurbanne Cedex, France*
[c] *FRAMATOME-ANP, 92084 Paris La défense Cedex, France*

Received 25 November 2004

Abstract

This work is concerned with the modeling of the thermal, metallurgical and mechanical phenomena encountered in the heat-affected zone (HAZ) during a welding operation. It focuses particularly on the analysis of models of thermo-mechanical behavior taking into account the metallurgical effects incorporated in the calculation code SYSWELD®. The studies were carried out on a 16MND5 low-alloy carbon manganese steel of the type used in the manufacturing of pressurized water reactor vessels for French nuclear power plants. These studies were based on specific one-dimensional tests of the ''Satoh'' type, which consist of austenitizing, then cooling homogeneously the useful portion of a test piece whose longitudinal displacements are restrained. In this case, virtually all thermo-mechanical and thermo-metallurgical phenomena observable in the HAZ are present simultaneously.

Keywords: Mechanical testing; Phase transformation; Transformation-induced plasticity; Cyclic loading

1. Introduction

A welding operation yields thermal, metallurgical and mechanical phenomena resulting in non-uniform strain and stress fields. These phenomena can affect the quality and the mechanical strength of the welded component dramatically. Therefore, the knowledge of the stress state is useful for damage evolution analysis. Uniaxial tests of the ''Satoh'' type can be used to induce all these observable phenomena in the HAZ.

* Corresponding author. Tel.: +33 4 72 43 83 33/87 87; fax: +33 4 72 43 85 78.
E-mail address: jean-francois.jullien@insa-lyon.fr (J.-F. Jullien).

0020-7683/$ - see front matter © 2004 Elsevier Ltd. All rights reserved.
doi:10.1016/j.ijsolstr.2004.11.018

Nomenclature

$\dot{E}^{pt}$	transformation plasticity strain rate
$\dot{E}^{cp}_{\Sigma}$	classical macroscopic plastic strain rate induced by a variation of the macrostress at constant temperature
$\dot{E}^{cp}_{T}$	classical macroscopic plastic strain rate induced by a temperature variation under constant stress
Σ^{eq}	macroscopic equivalent stress in the Von Mises' sense
Σ^{y}	homogenized limit stress
$\dot{\Sigma}^{eq}_{s}$	time derivative of the equivalent macrostress in the Von Mises' sense Σ'^{eq}, assuming the internal variable A_γ to be constant $\dot{\Sigma}^{eq}_{s} = \frac{3}{2\Sigma'^{eq}}(S - A_\gamma)\dot{S}$ $\Sigma'^{eq} = \left[\frac{3}{2}(S - A_\gamma)\cdot(S - A_\gamma)\right]^{\frac{1}{2}}$
S	macroscopic homogenized deviatoric tensor
σ^{y}_{γ}	elasticity limit of the austenitic phase
σ^{y}_{α}	elasticity limit of the ferritic phase
E^{eff}_{γ}	effective macroscopic isotropic strain hardening internal variable for the mother phase
E^{eff}_{α}	effective macroscopic isotropic strain hardening internal variable for the child phase
A_γ	macroscopic kinematic strain hardening internal variable for austenite
A	homogenized macroscopic kinematic strain hardening internal variable
E	Young's modulus, assumed to be the same for all phases
α_γ	thermal expansion coefficient of the austenitic phase
α_α	thermal expansion coefficient of the ferritic phase
$(1-z)$	Austenite proportion
z	child phase proportion
$f(z)$	corrector function based on numerical simulations
$g(z)$	corrector function based on numerical simulations
Tbf	initial temperature of the ferritic transformation
Tef	final temperature of the ferritic transformation
TbB	initial temperature of the bainitic transformation
Ms	initial temperature of the martensitic transformation
$\Delta\varepsilon^{th}_{\gamma\alpha}$	thermal strain difference between the two phases
$h\left(\frac{\Sigma^{eq}}{\Sigma^{y}}\right)$	term expressing the non-linear nature of transformation plasticity for a certain level of applied stress
θ	memory coefficient expressing the percentage of strain hardening transmitted from the mother phase to the child phase: $\theta = 1$ strain hardening transmission; $\theta = 0$ strain hardening recovery

This, along with the simplicity associated with the one-dimensional aspect, led us to choose this type of test in the framework of this study for the analysis of mechanical behavior models including metallurgical effects developed by Leblond and coworkers (Leblond et al., 1986a,b, 1989; Leblond, 1989) and implemented in the calculation code SYSWELD® (ESI).

Actually, many heuristic or micromechanically based models have been proposed for transformation-induced plasticity (TRIP) in context of welding analysis. Notable contributions are due, among others, to Abrassart (1972), Börjesson and Lindgren (2001), Cherkaoui et al. (1998), Fischer (1997), Fischer et al. (2000), Giusti (1981), Greenwood and Johnson (1965), Magee (1966), Mitter (1986), Ronda and Oliver (2000), Simon et al. (1994), Sjöström (1984), Videau et al. (1994), Wang and Inoue (1985). However, the model developed by Leblond and coworkers which stands as a refined extension of the seminal work of Greenwood and Johnson (1965), seems especially attractive for practical applications. Indeed, being based

on a micromechanical analysis relating transformation plasticity to ordinary plasticity at a smaller scale, it does not require any information from the user implying performing transformation plasticity experiments for the specific material considered, but the sole knowledge of usual thermo-mechanical parameters.

Uniaxial tests of the "Satoh" type were performed for the first time, as implied by its name, by Kunihiko Satoh nearly 30 years ago (Satoh, 1972a,b). In the literature, other teams (Itoh and Kashiwaya, 1992; Dupas, 1998) developed these tests further, sometimes improving them or comparing them with results from numerical simulations. The Satoh test involves only local phenomena: it consists of austenitizing, then cooling homogeneously the useful portion of a test piece whose longitudinal displacements are restrained (the useful portion being defined as the zone being measured within which the temperature and stress fields are homogeneous). Thus, the metallurgical transformations occur simultaneously at all points of the measured zone. Since the overall deformation is prescribed to be zero throughout the thermal cycle, an axial stress develops. Then, by comparing the evolutions of calculated and measured stresses, one can analyze, among other phenomena, those related to transformation-induced plasticity, relief from strain hardening and the particular behavior of phase mixtures. First, we will describe the experimental setup. Then, we will present, based on its capabilities, the experimental procedures introduced to carry out the tests. Finally, we will perform a comparative analysis of the calculations vs. the experiment.

2. Experimental method

Carrying out tests of the Satoh type required the design of a specific experimental device (Cavallo, 1998) consisting of a dilatometer enabling us to perform thermal and mechanical tests simultaneously. The test pieces were tubes made of low-alloy ferritic steel of the 16MND5 type (AFNOR Norm, see Table 1). The geometry and dimensions were defined such that the temperature field would be homogeneous over the whole measured zone (Fig. 2). This zone was compatible with the heating and cooling systems and presented a sufficient volume for the macroscopic behavior to be represented correctly.

The test pieces were heated by Joule effect. This volume heating process was chosen in order both to minimize the temperature gradients across the thickness of the test piece and to enable strain and temperature measurements to be performed in the useful zone of the test piece. This setup enabled rates of temperature increase on the order of 100 °C/s up to a maximum temperature greater than 1100 °C. During the cooling stage, at low-cooling rates, heat input by Joule effect was required. At higher rates, cooling was forced by a flow of nitrogen inside the test piece. These two processes provided rates of temperature decrease between −0.1 °C/s and −15 °C/s. The high-temperature use of nitrogen helped control the oxidation of the inner surface of the test piece. A flow of argon was applied on the external surface (Fig. 1). The thermal cycles were driven by an EUROTHERM programmer/controller. The temperature measurements were performed using thermocouples microwelded on the external surface of the test piece. Several thermocouples were used to ensure that the temperature in the useful zone was uniform along the axis. The mechanical loading device allowed prescribed-force and prescribed-strain cycles to be carried out (Fig. 3). The loading consisted of uniaxial traction or compression applied via a 100 kN servo-hydraulic jack. During a Satoh test, because of the temperature rise and metallurgical transformations, the characteristics of the material

Table 1
Chemical composition of the 16MND5 steel being studied

	C	Si	Mn	Ni	Cr	Mo	Al	Sn	S	P	N
Min	0.196	0.22	1.51	0.63	0.19	0.51	0.021	< 20 ppm	< 0.002	< 0.002	< 0.004
Max	0.212	0.23	1.58	0.65	0.20	0.53	0.024				

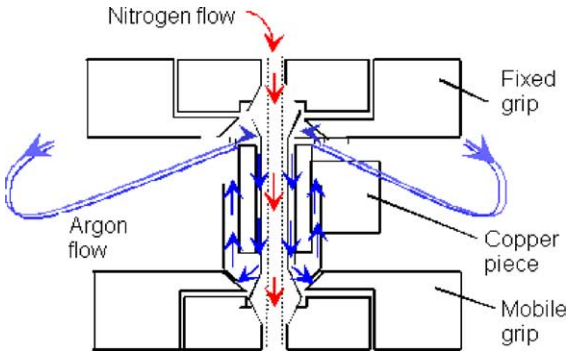

Fig. 1. Diagram of the cooling system by forced gas flow.

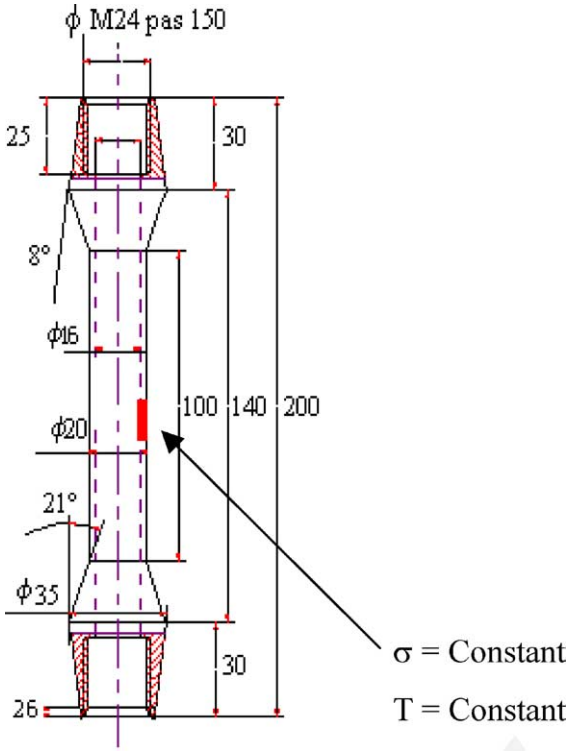

Fig. 2. Geometry of the test pieces.

evolve, which requires an automated adaptation of the regulation parameters in order to control the load in terms of both force and displacement. The new system we developed (Vincent, 2002) enables continuous auto-adaptation of the proportional terms. Repeatability is preserved even if the response of the test piece being studied presents rapid variations during a cycle, which is the case in a "Satoh" test involving metallurgical transformations.

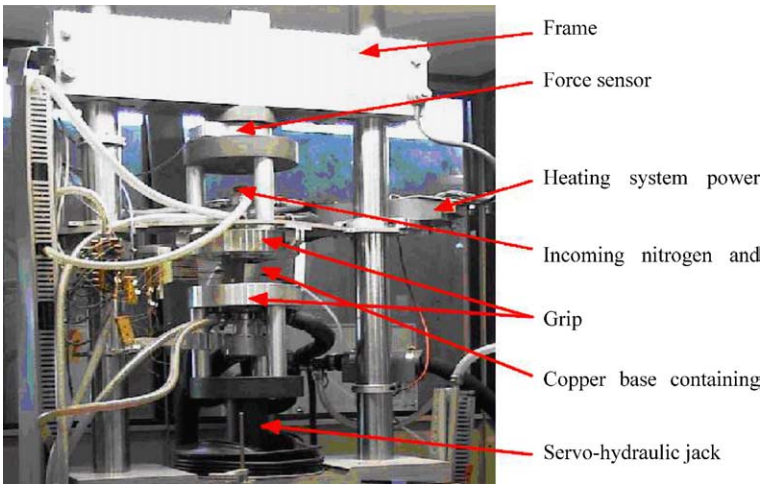

Fig. 3. General view of the testing apparatus.

3. The test program

The test program was designed in such a way that all thermal, metallurgical and mechanical phenomena occurring in the HAZ during a welding operation would be present. However, a precise knowledge of the thermo-metallurgical and mechanical characteristics of the metallurgical constituents being studied is necessary in order to interpret the test results and derive a detailed comparison with the calculations. In addition, other tests were included besides Satoh tests: traction–compression tests at a fixed strain rate ($\dot{\varepsilon} = 0.00025/s$) and different temperatures in order to measure the basic mechanical characteristics of the different possible material structures and free dilatometer tests (Vincent, 2002) performed just prior to the Satoh test and on the same test piece to minimize the dispersion of the experimental results. The latter tests enabled us to identify the expansion characteristics and the volume changes produced by the metallurgical transformations in terms of the austenitization parameter being considered.[1] Three types of tests were conducted:

- The first type corresponds to thermal evolutions yielding complete and unique metallurgical transformations during heating and cooling. The transformations considered during cooling were the bainitic and martensitic transformations.
- The second type corresponds to thermal evolutions yielding double transformations during cooling. These are the ferritic–bainitic and bainitic–martensitic transformations.
- The final, very specific type corresponds to thermal evolutions yielding only partial austenitization during heating. The maximum temperature reached lies within the dynamic austenitic transformation range.

For the first two types of tests, we considered repeated thermal cycles with decreasing maximum temperatures. These cycles were performed in order to gather information on certain effects related to multipass welding. The heating rate was prescribed at 80 °C/s. During the first two thermal cycles, the maximum tem-

[1] During austenitization, two parameters play an essential role: the maximum temperature reached and the time during which the temperature remains above the initiation temperature of the austenitic transformation Ac'1. These two parameters determine the austenitization parameter, which represents an equivalence between time and temperature.

peratures reached were 1100 °C and 900 °C respectively. These were greater than the dynamic temperature at the end of austenitic transformation (Ac'3 ≅ 850 °C). The cooling temperatures were controlled between 800 °C and the ambient temperature. These were identical for the first two cycles, but varied from one test to the next depending on the type of metallurgical transformation desired. For the last two cycles, the maximum temperatures reached were 670 °C and 400 °C respectively, which is less than the initial dynamic temperature of the austenitic transformation (Ac'1 ≅ 735 °C).

For the last type of Satoh test, the prescribed heating and cooling rates were close to 12 °C/s. For the austenitization parameter being considered, such a cooling rate enables one to prevent ferritic transformation to occur and to minimize the percentage of bainitic phase generated. Thus, a multiphase mix containing austenite is present between the final temperature of the heating stage and the temperature at the end of the martensitic transformation.

4. The numerical analysis

4.1. Thermo-metallurgical formulation

Thermal properties are phase dependent, and metallurgical transformations involve latent heats; conversely, transformations of course depend on temperature. Thus the thermal and metallurgical calculations are fully coupled and performed simultaneously. The heat conduction equation is solved using an enthalpic formulation (Bergheau and Leblond, 1991) especially fit for optimal numerical treatment of latent heat effects. However, both the evolution of temperature in the useful zone (which results from Satoh tests) and the kinetics of the metallurgical transformations (which results from free dilatometer tests) are known. Thus, the thermo-metallurgical calculation is not a calculation in the strict sense because the temperatures and the kinetics of the transformations are prescribed. Therefore, the results of the thermo-metallurgical calculations are merely data for the next step, which is the mechanical calculation.

4.2. Thermo-mechanical formulation

The calculations involved here are elastic–plastic calculations in large strain (based on an updated Lagrangian formulation). We chose Von Mises' plasticity criterion, whose evolution (kinematic or isotropic) depends on the type of calculation envisaged. For calculations using an isotropic strain hardening law, we chose the proportionality limit as the elastic limit. For kinematic calculations, the elastic limit was set conventionally to 0.2% plastic strain. In either case, strain hardening was considered non-linear. Both the influence of mechanics on thermics by intrinsic dissipation and the influence of metallurgy on thermics by heat absorption or release during the metallurgical transformation (the transformation's latent heat phenomenon) were taken into account implicitly by prescribing the measured temperature.

In SYSWELD, the total strain is partitioned as follows:

$$E^{t} = E^{e} + E^{thm} + E^{pc} + E^{pt}$$

where E^{e} is the macroscopic elastic strain, E^{thm} is the macroscopic thermo-metallurgical strain, E^{pc} is the classical macroscopic plastic strain and E^{pt} is the transformation-induced-plasticity strain.

4.2.1. The macroscopic thermo-metallurgical strain

Solid-state phase changes are characterized by geometric transformations of the crystal lattice. Austenite is a solid solution inserted in γ iron, whereas the ferritic phases are solid carbon solutions inserted in α iron. Due to their geometric characteristics, these two types of crystalline structures have different densities which result, on the macroscopic level, in a so-called transformation-induced volumetric strain. This volume

change associated with thermal dilatation and contraction defines the so-called thermo-metallurgical transformation strain. This isotropic quantity from a macroscopic standpoint was determined from free dilatometer tests (Vincent, 2002; Taleb, 1998):

$$E^{\mathrm{thm}}(T,z) = (1-z)\varepsilon_{\gamma}^{\mathrm{th}}(T) + z\cdot\varepsilon_{\alpha}^{\mathrm{th}}(T)$$

$$\varepsilon_{\alpha}^{\mathrm{th}}(T) = \alpha_{\alpha}\cdot[T - T_{\mathrm{ref}}]$$

$$\varepsilon_{\gamma}^{\mathrm{th}}(T) = \alpha_{\gamma}\cdot[T - T_{\mathrm{ref}}] - \Delta\varepsilon_{\alpha\gamma}^{25\ ^{\circ}\mathrm{C}}$$

where: $T_{\mathrm{ref}} = 25\ ^{\circ}\mathrm{C}$.

Thermal strain difference between the two phases: $\Delta\varepsilon_{\alpha\gamma}^{25\ ^{\circ}\mathrm{C}} = 0.01$.

Thermal expansion coefficient of the austenitic phase ($T_{\mathrm{ref}} = 1000\ ^{\circ}\mathrm{C}$):

$$\alpha_{\gamma} = 22.6\times10^{-6} + 2.52\times10^{-9}\cdot T$$

Thermal expansion coefficient of the ferritic phase ($T_{\mathrm{ref}} = 25\ ^{\circ}\mathrm{C}$):

$$\begin{array}{ll} T < 350\ ^{\circ}\mathrm{C} & \alpha_{\alpha} = 12.35\times10^{-6} + 7.710^{-9}\cdot\ T \\ 350\ ^{\circ}\mathrm{C} < T < 700\ ^{\circ}\mathrm{C} & \alpha_{\alpha} = 15\times10^{-6}\ ^{\circ}\mathrm{C}^{-1} \end{array}$$

4.2.2. Classical plastic strain and transformation-induced plasticity strain

The models implemented in SYSWELD to describe the mechanical behavior of elastic–perfectly plastic materials are presented in (Leblond et al., 1986a,b, 1989). The extension of these models to materials with isotropic or kinematic strain hardening is described in (Leblond, 1989).

Leblond considers a mixture of austenite (phase γ) with volume fraction $1-z$ and ferrite, bainite or martensite (phase α) with volume fraction z, and assume that phase γ is being transformed into phase $\alpha(\dot{z}>0)$. The results of the homogenization process are as follows. Following Leblond et al. (1989), one distinguishes between two regimes according to whether the macroscopic equivalent stress Σ^{eq} does or does not reach the "ultimate" stress Σ^{y} of the mixture given by

$$\text{Isotropic formulation}: \Sigma^{y} = [1-f(z)]\cdot\sigma_{\gamma}^{y}(E_{\gamma}^{\mathrm{eff}}) + f(z)\cdot\sigma_{\alpha}^{y}(E_{\alpha}^{\mathrm{eff}})$$

$$\text{Kinematic formulation}: \Sigma^{y} = [1-f(z)]\cdot\sigma_{\gamma}^{y} + f(z)\cdot\sigma_{\alpha}^{y}$$

In the first expression E_i^{eff} is the average hardening parameter of phase i. The quantity E_i^{eff} governing strain hardening here differs from the usual cumulated equivalent plastic strain E_i^{eq} because of possible recovery of hardening during transformations. A linear mixture law is used for a ferritic phases mixture and a non-linear one for a austenite–ferritic mixture. The non-linearity intervenes through a function $f(z)$ depending on the proportions of ferritic phases z. The function $f(z)$ have been deduced from the numerical simulation (Leblond et al., 1986b and Devaux, 1998). Indeed, this stress is not relative to the first occurrence of plasticity because plasticity exists even in the absence of external stress due to the internal stresses induced by the difference of densities between the austenitic phase and the ferritic phases. Thus, a distinction is made between two plastic flow regimes.

If $\Sigma^{\mathrm{eq}} = \Sigma^{y}$, plastic flow occurs in both phases (global yield). No detailed treatment of microscopic mechanisms is necessary in this case. It is sufficient to state that the macroscopic plastic strain rate is positively collinear to the macroscopic stress deviator and that the evolutions of the average hardening parameters are governed by the following equations (Leblond, 1989):

Isotropic hardening

$$\dot{E}_{\gamma}^{\mathrm{eff}} = \dot{E}^{\mathrm{eq}} \quad \dot{E}_{\alpha}^{\mathrm{eff}} = \dot{E}^{\mathrm{eq}} + \frac{\dot{z}}{z}\left(-E_{\alpha}^{\mathrm{eff}} + \theta E_{1\gamma}^{\mathrm{eff}}\right)$$

Kinematic hardening

$$\dot{B}_\gamma = \dot{E}^{\mathrm{p}} \quad \dot{B}_\alpha = \dot{E}^{\mathrm{p}} - \frac{\dot{z}}{z} B_\alpha + \theta \frac{\dot{z}}{z} B_\gamma$$

where θ is a parameter governing possible recovery of strain hardening during the transformation.

If the macroscopic equivalent stress, in Von Mises' sense, is less than this homogenized limit stress ($\Sigma^{\mathrm{eq}} < \Sigma^y$), the total plastic deformation is composed of two terms, the classical term $\dot{E}^{\mathrm{p}}_{\mathrm{cp}}$ plus an additional, so-called transformation-induced plasticity (TIP) term $\dot{E}^{\mathrm{p}}_{\mathrm{tp}}$. Thus, below the macroscopic plasticity limit Σ^y, a classical plastic flow may occur and the behavior of the multiphase mix containing austenite is taken into account through the presence of an additional classical plastic strain term $\dot{E}^{\mathrm{p}}_{\mathrm{cp}}$. This term is function of the variation of macroscopic stress and of the variation of temperature. The transformation-induced plasticity results from the coupling between an external stress and the evolution of the proportions of the existing phases. Indeed, the application of even a small stress during the transformation yields an additional strain besides the metallurgical volumetric strain in the direction of the applied stress. Leblond developed a multiaxial and incremental formulation of the transformation-induced plasticity strain. The choice of a model to represent this phenomenon was based on a theoretical as well as numerical study of Greenwood and Johnson's mechanism (Greenwood and Johnson, 1965); Magee's mechanism (Magee, 1966) was neglected. This transformation-induced plasticity strain rate is proportional to the applied stress, to the volume variation associated with the phase change and to the progress of the transformation, but inversely proportional to the elastic limit of the softest phase.

Isotropic formulation

$$\dot{E}^{\mathrm{cp}} = \frac{3(1-z)}{2\sigma^y_\gamma(E^{\mathrm{eff}}_\gamma)} \cdot \frac{g(z)}{E} \cdot S \cdot \dot{\Sigma}^{\mathrm{eq}} + \frac{3(\alpha_\gamma - \alpha_\alpha)}{\sigma^y_\gamma(E^{\mathrm{eff}}_\gamma)} z \cdot \ln z \cdot S \cdot \dot{T}$$

$$\dot{E}^{\mathrm{pt}} = -\frac{\Delta V/V}{\sigma^y_\gamma(E^{\mathrm{eff}}_\gamma)} \cdot S \cdot h\left(\frac{\Sigma^{\mathrm{eq}}}{\Sigma^y}\right) \cdot (\ln z) \cdot \dot{z}$$

The evolution equations for the hardening parameters of the phases are given by

$$\dot{E}^{\mathrm{eff}}_\gamma = \frac{\dot{E}^{\mathrm{eq}}}{1-z} \qquad \dot{E}^{\mathrm{eff}}_2 = -\frac{\dot{z}}{z} E^{\mathrm{eff}}_2 + \theta \frac{\dot{z}}{z} E^{\mathrm{eff}}_1$$

Kinematic formulation

$$\dot{E}^{\mathrm{cp}} = \frac{3(1-z)}{2\sigma^y_\gamma} \cdot \frac{g(z)}{E} \cdot (S - A_\gamma) \cdot \dot{\Sigma}^{\mathrm{eq}}_{\mathrm{s}} + \frac{3(\alpha_\gamma - \alpha_\alpha)}{\sigma^y_\gamma} z \cdot \ln z \cdot (S - A_\gamma) \cdot \dot{T}$$

$$\dot{E}^{\mathrm{pt}} = -\frac{\Delta V/V}{\sigma^y_\gamma} (S - A_\gamma) \cdot h\left(\frac{\Sigma^{\mathrm{eq}}}{\Sigma^y}\right) \cdot (\ln z) \cdot \dot{z}$$

The evolution equations for the hardening parameters of the phases are given by

$$\dot{B}_\gamma = \frac{\dot{E}^p}{1-z} \qquad \dot{B}_\alpha = -\frac{\dot{z}}{z} B_\alpha + \theta \frac{\dot{z}}{z} B_\gamma$$

In these equations, E denotes Young's modulus (supposedly identical for both phases), S_{ij} the macroscopic stress deviator, α_i the heat expansion coefficient of phase i and $\Delta V/V$ the change of specific volume accompanying the transformation (i.e. the trace of the transformation strain). The functions g, and h in these equations have been given in (Leblond et al., 1986b).

4.2.3. Strain hardening recovery

The strain hardening recovery phenomenon is simply the possible non-transmission of strain hardening from the mother phase to the product phase. This phenomenon was described by Leblond from a mechanical standpoint by introducing two strain hardening parameters—one for the child phase and one for the mother phase—instead of a single, global one. The evolution laws on the internal strain hardening variables are different from the usual laws in order to enable the return of these parameters to zero during transformations. The strain hardening recovery phenomenon is taken into account through a memory coefficient θ such that the new internal variable of the phase produced on the transformation's front equals that of the mother phase multiplied by this memory coefficient θ. Memory is inexistent if $\theta = 0$ and complete if $\theta = 1$ (Leblond, 1989, 1990).

5. Test results and comparative analysis

We will present and comment the experimental and numerical results in the following test cases:

- Satoh 0.3: Satoh test with a prescribed cooling rate of 0.3 °C/s. The first thermal loading stage generates a completely bainitic transformation during cooling and the second, a double ferritic–bainitic transformation (Fig. 4).
- Satoh 12: Satoh test with a prescribed cooling rate of 12 °C/s. The first thermal loading stage generates a completely martensitic transformation during cooling and the second, a double bainitic–martensitic transformation (Fig. 5).
- Satoh ZPAT: Satoh test with only partial austenitic transformation during heating. The cooling rate was set to 12 °C/s. This thermal loading generates a double bainitic–martensitic transformation during cooling (Fig. 6).

5.1. Test results

5.1.1. Cooling rate and austenitization parameter

For a given austenitization parameter, the cooling rate governs both the type and the kinetics of the structural transformation. The higher the cooling rate, the lower the temperatures at which the transformation starts and ends. These metallurgical transformations are accompanied by a volume expansion which counteracts the thermal contraction. Thus, different evolutions of stresses occur depending on the cooling rate. Generally, the higher the temperature at the end of the transformation, the higher the traction stress upon return to ambient temperature. The stress at ambient temperature may or may not exceed the elastic limit of the metallurgical constituent present. The time during which the temperature is maintained above the equilibrium temperature of the beginning of the austenitic transformation and the maximum temperature reached determine the austenitization parameter. The higher this parameter, the larger the austenitic grain. Since this grain size has great influence on the transformations occurring during cooling, the evolution of stresses is different in the first and second thermal cycles, even though the cooling rates are identical. Rapid austenitization conditions with smaller holding times tend to favor high-temperature transformations.

Finally, the results show a direct relationship between the thermo-mechanical characteristics of the austenitic phase and the austenitization parameter. The evolution of the tension stress between the maximum temperature reached and the temperature at the beginning of the transformation during cooling is different in the first and in the second cycle. This evolution depends on the austenitic grain size: the smaller grain size in the second thermal cycle yields a greater resistance to traction.

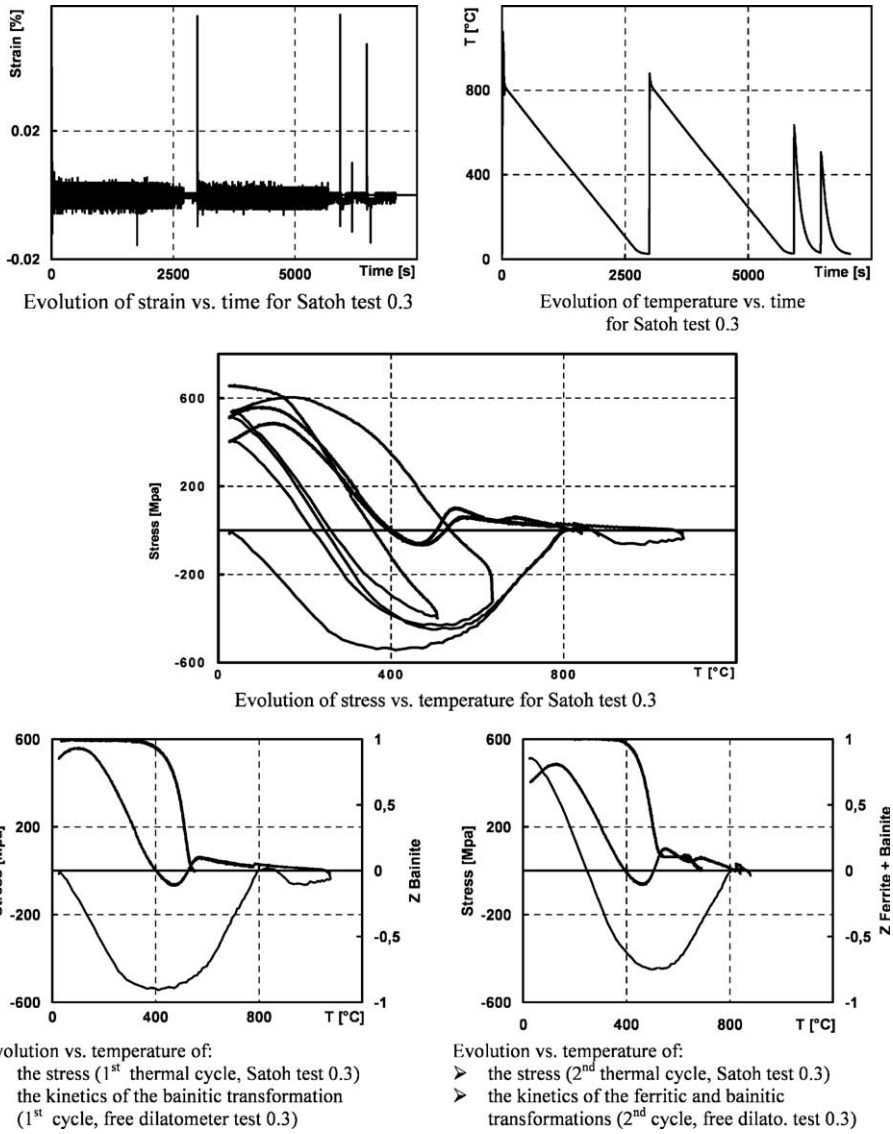

Fig. 4. Experimental results for Satoh test 0.3.

5.1.2. Applied load

The phase transformation kinetics was determined from free dilatometer tests just prior to the Satoh test and on the same test piece. Thus, this determination was conducted under zero loading. However, several experimental works have shown that the transformation's characteristics can be influenced by the application of a uniaxial stress (Gautier, 1985; Denis, 1987; Simon et al., 1994). During a Satoh test, the stress is practically never zero. Therefore, by comparing the temperature of stress release of the Satoh test with the temperature at the beginning of the transformation determined by the free dilatometer test, we can observe, based on the Table 2, a significant increase in the initial temperatures of the martensitic ($\Delta T = 56\ ^\circ C$) and bainitic ($\Delta T = 25\ ^\circ C$) transformations in the case of complete transformations under stress. Therefore,

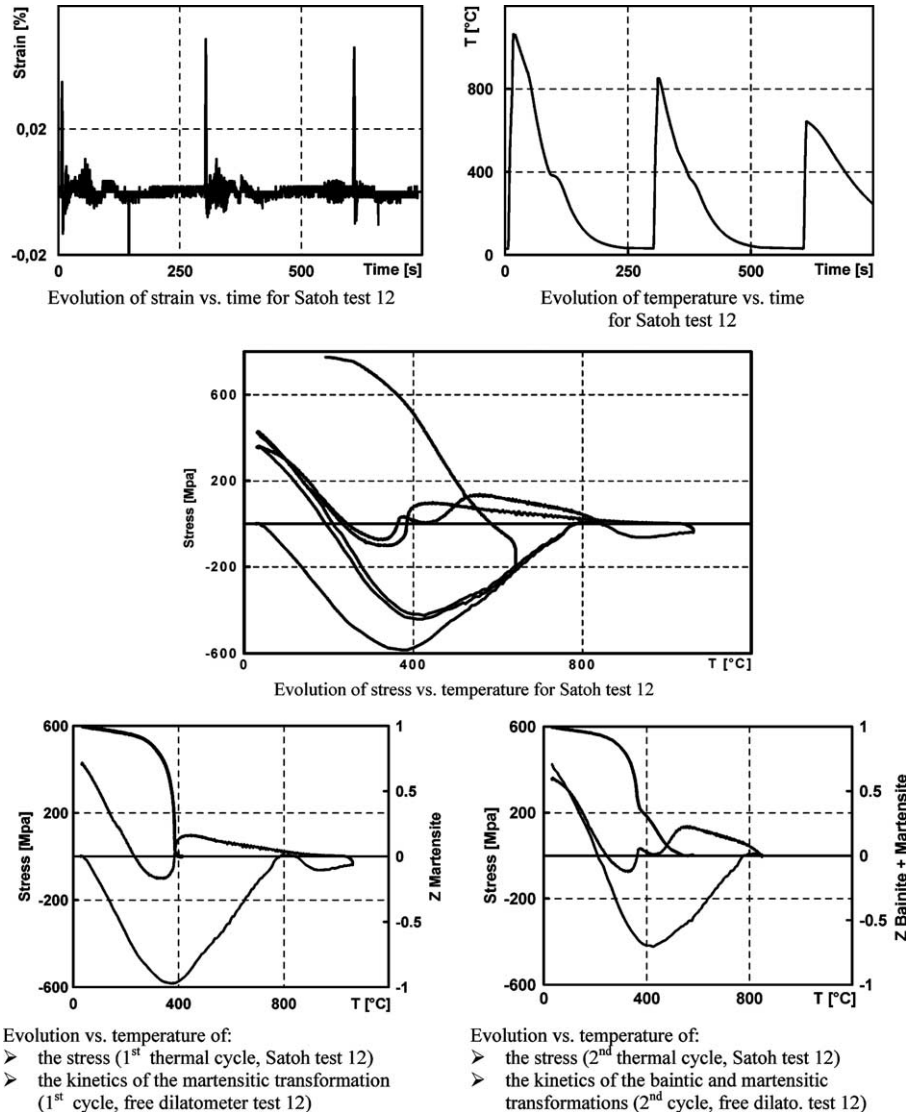

Fig. 5. Experimental results of Satoh test 12.

overall, these observations confirm the results of the works in the literature, i.e. the fact that a uniaxial solicitation may induce the metallurgical transformation.

5.1.3. Viscoplasticity

Viscoplastic behavior occurs in virtually all metals and alloys operating at high temperature. It is a result of the influence of time (and, therefore, the influence of the loading rate) on the permanent deformations and stress state. This effect is particularly noticeable during the third thermal cycles at the end of heating and at the beginning of cooling for temperatures between 600 °C and 700 °C. Significant relaxation of the compression stress by viscoplastic flow can be observed in all test cases.

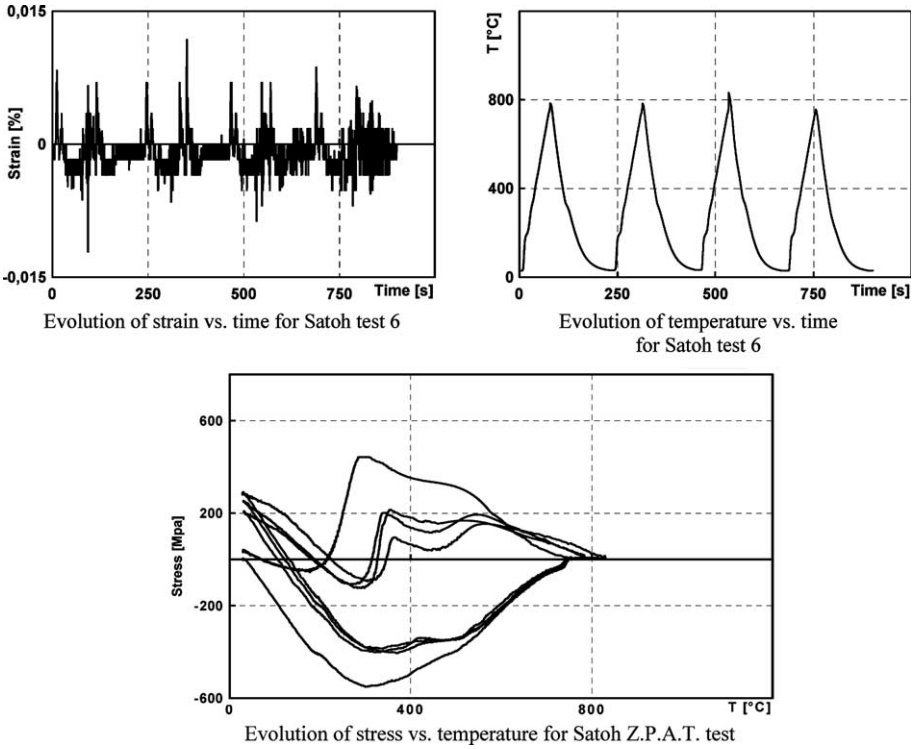

Fig. 6. Experimental results of Satoh ZPAT test.

Table 2
Initial transformation temperatures at cooling determined by free dilatometer tests and Satoh tests (Ap: austenitization parameter)

Test	Dilato 0.3			Satoh 0.3		
T (°C)	TbF	TbB	Ms	TbF	TbB	Ms
$Ap_{(1100)}$		545 °C			570 °C	
$Ap_{(900)}$	689 °C	540 °C		690 °C	554 °C	
Test	Dilato 12			Satoh 12		
T (°C)	TbF	TbB	Ms	TbF	TbB	Ms
$Ap_{(1100)}$			399 °C			455 °C
$Ap_{(900)}$		541 °C	372 °C		556 °C	373 °C

5.1.4. Partial austenitization

Fig. 6 shows the evolution of the axial stress against the temperature for the Satoh ZPAT test. Four successive thermal cycles were applied. They differ very slightly from one another in terms of the maximum temperature reached (cf. Table 3). Let us again point out that this test case is very specific in that the thermal loading generates only partial austenitization during heating, which leads to a multiphase mix containing austenite during cooling.

Four remarkable points are worth noting:

- The stress upon return to ambient temperature diminishes with the maximum temperature reached and, therefore, with the percentage of austenitic phase generated.

Table 3
Maximum temperature reached,percentage of austenitic phase generated during heating and stress at ambient temperature

Satoh ZPAT	1st Cycle	2nd Cycle	3rd Cycle	4th Cycle
Maximum temperature [°C]	784	783	830	756
Stress release temperature [°C]	354	341.5	361.5	284.8
Stress level before release [Mpa]	213.9	201.9	94.8	442.5
Stress at ambient temperature [Mpa]	252	207	285	33

- The lower the temperature at the end of heating, the lower the temperature of stress release at the beginning of the martensitic transformation.
- The smaller the percentage of austenitic phase transformed during heating, the higher the stress level prior to the martensitic transformation. The traction stress just prior to the martensitic transformation in the 4th cycle was 442.4 Mpa, which is much greater than the limit stress of austenite at this temperature.
- The smaller the proportion of austenitic phase generated during heating, the larger the drop in traction stress generated by the martensitic transformation during cooling.

5.2. Comparative analysis

Let us compare the results from kinematic and isotropic calculations and the experimental measurements for Satoh test cases 0.3 and 12 (Figs. 7–13). The comparative analyses concern the constitutive relations (kinematic or isotropic), the transformation-induced plasticity phenomenon and the strain hardening recovery phenomenon.

5.2.1. Constitutive relations

The two constitutive relations yield somewhat different results, whether metallurgical transformations are present or not.

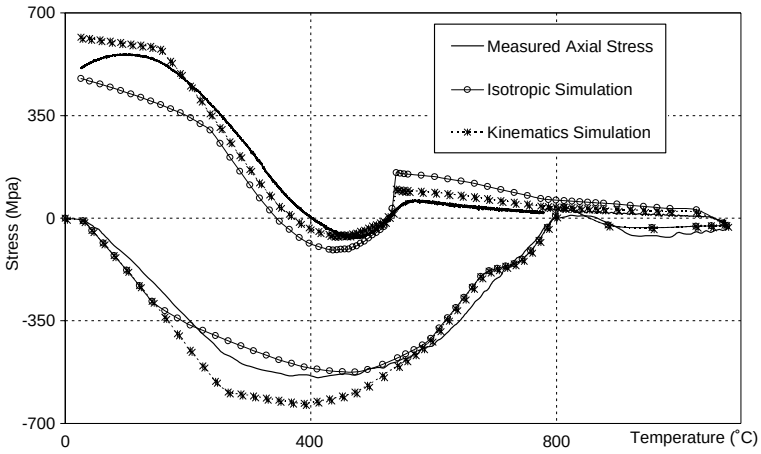

Fig. 7. Comparison between experimental results and numerical simulations Satoh test 0.3 first thermal cycle.

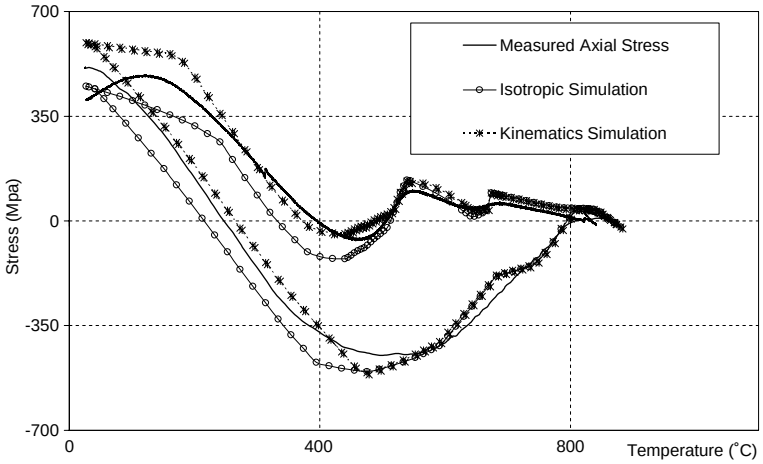

Fig. 8. Comparison between experimental results and numerical simulations Satoh test 0.3 second thermal cycle.

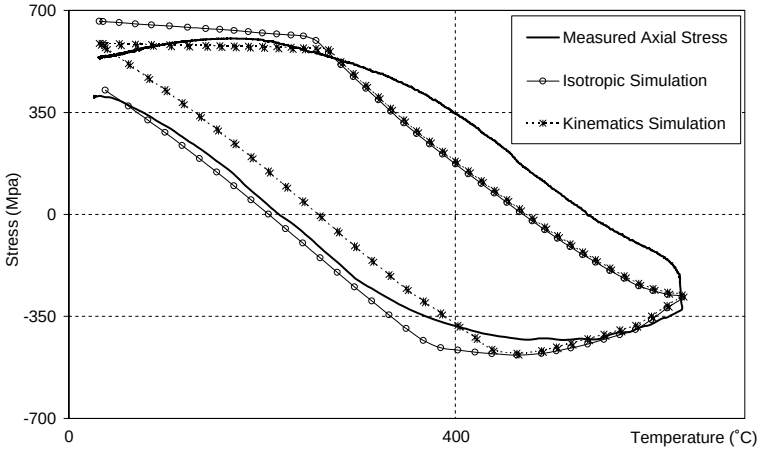

Fig. 9. Comparison between experimental results and numerical simulations Satoh test 0.3 third thermal cycle.

Case of high stresses: $\Sigma^{eq} = \Sigma^{y}$:

This configuration occurs particularly in the absence of phase transformation. The dominant factors are associated with the classical strain hardening law: isotropic strain hardening by simple dilatation results in excessive final stresses and even in complete elastic adaptation after four cycles in Satoh test case 0.3.

The constitutive relation with kinematic strain hardening uses a conventional elasticity limit at 0.2% plastic strain. The first and obvious drawback is that the first stages of plastic strain are not taken into account correctly. However, the Bauschinger effect is approximately represented.

Case of low stresses: $\Sigma^{eq} < \Sigma^{y}$:

This configuration occurs whenever metallurgical transformations take place during cooling. The volume expansion which coincides with the metallurgical transformation counteracts the thermal contraction. The additional plastic flow induced by the classical plastic strain and the transformation-induced plasticity strain also tends to reduce the elastic strain and, consequently, the stress. For small stresses, the differences between the isotropic and kinematic constitutive relations lie in the definitions of the classical macroscopic

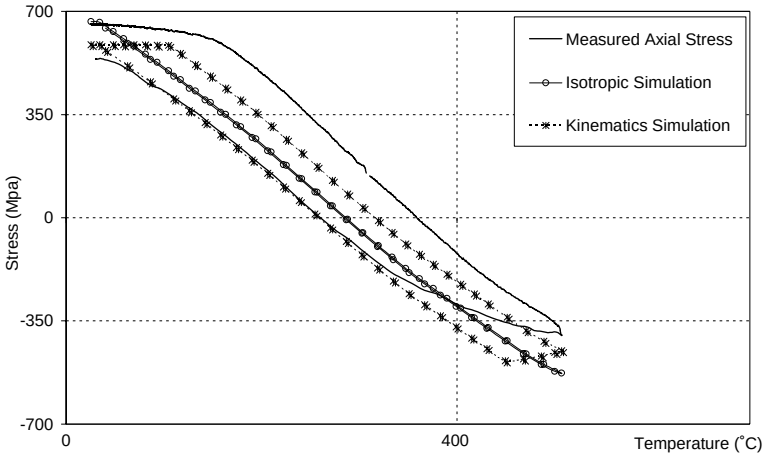

Fig. 10. Comparison between experimental results and numerical simulations Satoh test 0.3 fourth thermal cycle.

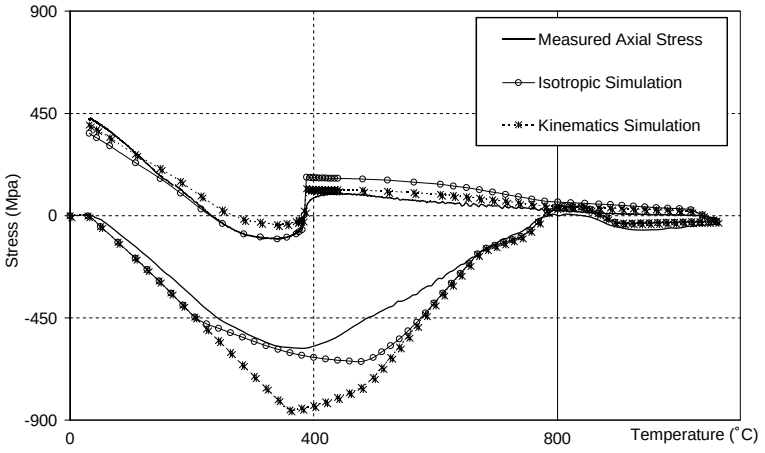

Fig. 11. Comparison between experimental results and numerical simulations Satoh test 12 first thermal cycle.

plastic strain rate and of the transformation-induced plasticity strain rate. These two strain rates are inversely proportional to the elastic limit of the mother phase.

Thus, the first difference between the two formalisms lies in whether or not the elastic limit of the mother phase depends on the effective macroscopic isotropic strain hardening internal variable of the austenitic phase E_γ^{eff}. If one takes this dependency into account by updating the elastic limit of the parent phase according to its strain hardening level, one reduces the influence of transformation-induced plasticity. This is one of the reasons why the stress release is greater when the isotropic formalism is used.

The second difference lies in the presence or absence in the definitions of the classical plastic strain rate and transformation-induced plasticity strain rate of an internal tensor variable A_γ which is subtracted from the deviatoric tensor of macroscopic stresses. Thus, the effective stress, rather than the nominal stress, determines the flow's direction. The variable $A_{\gamma 22}$ remains positive when the transformations occur during cooling. The stress σ_{22} is positive at the beginning of the transformation, then negative starting from a certain percentage of transformed phase because of the volume expansion associated with the transformation.

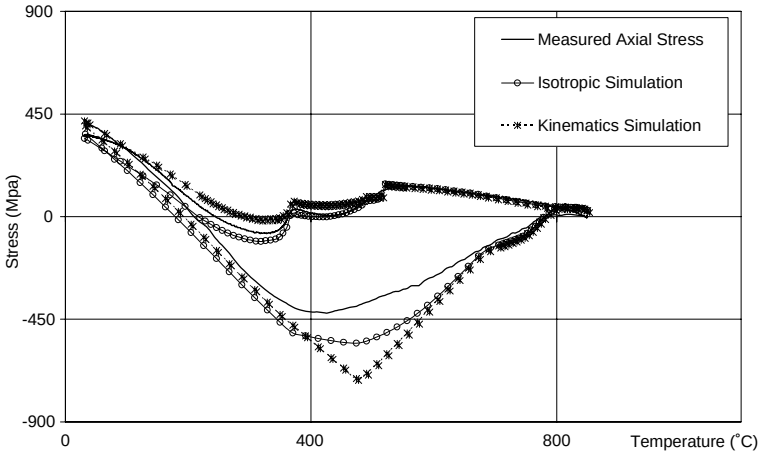

Fig. 12. Comparison between experimental results and numerical simulations Satoh test 12 second thermal cycle.

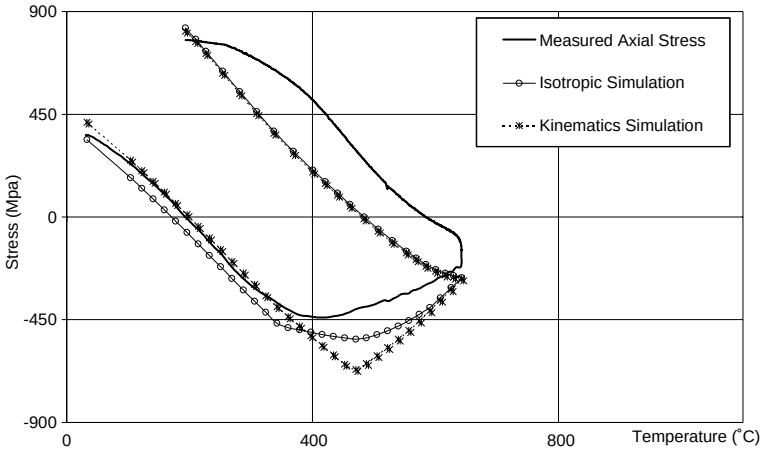

Fig. 13. Comparison between experimental results and numerical simulations Satoh test 12 third thermal cycle.

Thus, as long as the stress σ_{22} is positive, the quantity $S_{22} - A_{\gamma 22}$ is less than S_{22}. The influence of the classical plastic strain and transformation-induced plasticity strain is greater when the isotropic formalism is being used. Therefore, this formalism generates a faster stress reduction. Subsequently, the stress σ_{22} becomes negative and the quantity $S_{22} - A_{\gamma 22}$ is greater than S_{22} in absolute value. This time, the influence of the classical plastic strain and transformation-induced plasticity strain is greater when the kinematic formalism is being used. Thus, as soon as the stress turns to compression, the additional flow induced by the two strain rates tends to reduce the stress level, this consequence being more pronounced when the kinematic strain hardening constitutive relation is being considered.

While the kinematic calculation tends to underestimate the stress decrease during the metallurgical transformation, the isotropic calculation overestimates it. Therefore, a transformation-induced plasticity law associated with mixed isotropic–kinematic strain hardening could provide a better representation of the behavior of the steel being studied.

Remark: the martensitic transformation is carried out by displacive nucleation. The mechanisms used to explain the transformation-induced plasticity phenomenon are Greenwood and Johnson's mechanism and

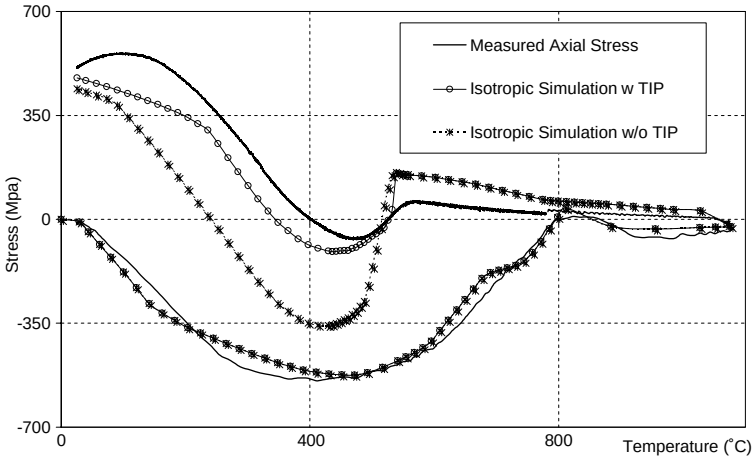

Fig. 14. Comparison between experimental results and numerical simulations with and without TIP effect Satoh test 0.3 first thermal cycle.

Magee's mechanism. While the former provides a good representation of the phenomenon occurring during diffusion transformations, it is generally thought that the latter, which takes into account the orientation of the zones transformed by external stresses, dominates when the transformation is athermal martensitic. However, although we indicated that Magee's mechanism was neglected in the calculations, the comparative results remained very good. Therefore, the idea that Magee's mechanism dominates over Greenxood and Johnson's mechanism in a martensitic transformation is questionable.

5.2.2. Transformation-induced plasticity strain

It is generally accepted today that the additional flow induced by the so-called transformation-induced plasticity strain plays a significant role in the evolution of the stress during structural transformations occurring in ferrous alloys. We can also verify this point. Indeed, when metallurgical transformations occur

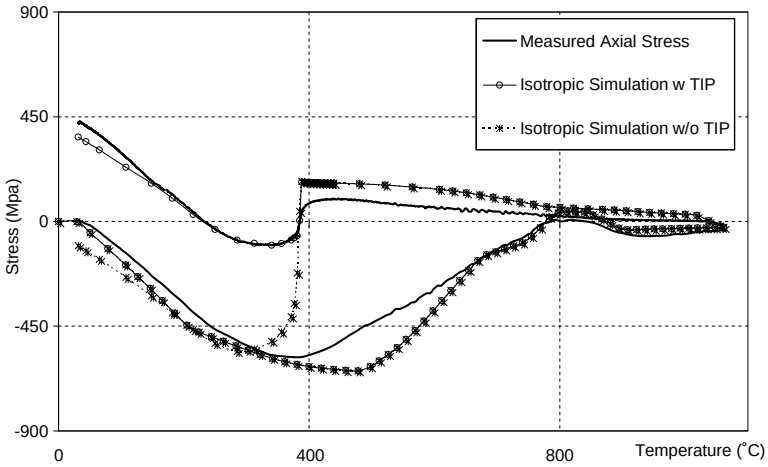

Fig. 15. Comparison between experimental results and numerical simulations with and without TIP effect Satoh test 12 first thermal cycle.

during cooling, the transformation-induced plasticity strain does tend to bring the stress back near the zero-stress state. Without transformation-induced plasticity the stress decreases more rapidly and the differences between the calculated results and experimental measurements are greater (Figs. 14 and 15). Quantitatively, toward the end of the bainitic transformation ($T \cong 400$ °C: Satoh 0.3), one observes a difference of 250 Mpa between the two calculations for the first cycle.

Back to ambient temperature, regardless of the cycle considered, the differences among the stress values obtained from the two calculations and the experimental values are small. The elastic limit of the monophasic or multiphasic material obtained has been reached, which yields to plastification before the end

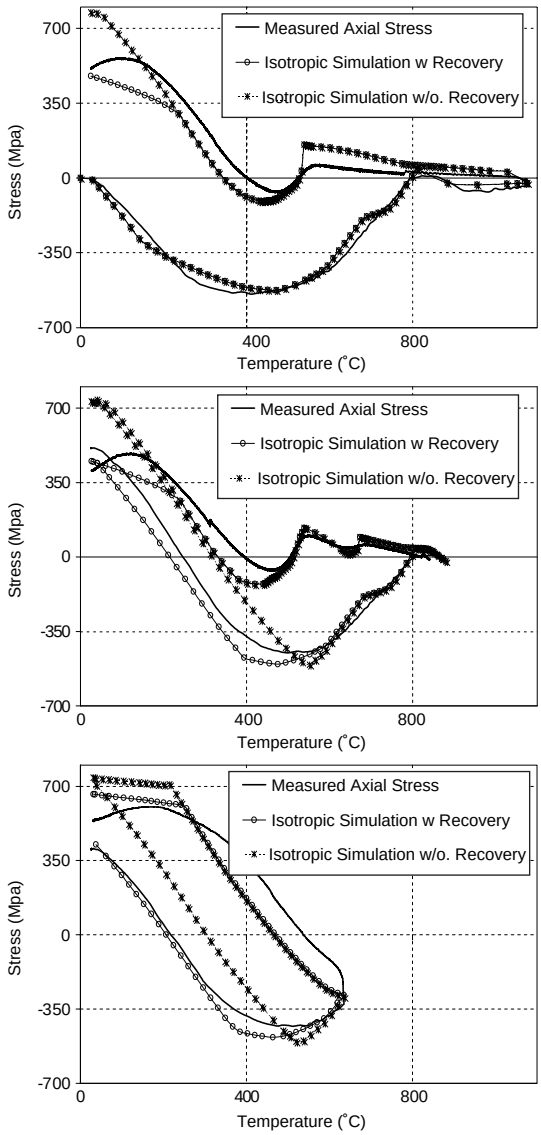

Fig. 16. Comparison between experimental results and numerical simulations with and without strain hardening recovery Satoh test 0.3.

of cooling. Therefore, one can stress the fact that a correct level of residual stresses is no guarantee that the phenomena occurring during structural transformations have been modeled correctly. Indeed, plastification resulting from these transformations can partially obliterate their mechanical effects and, consequently, the lack of precision associated with the way these are accounted for.

5.2.3. Strain hardening recovery

We will study this phenomenon by presenting simultaneously the results of an isotropic calculation with and without taking strain hardening transmission into account (Figs. 16 and 17). In Satoh test 0.3, during

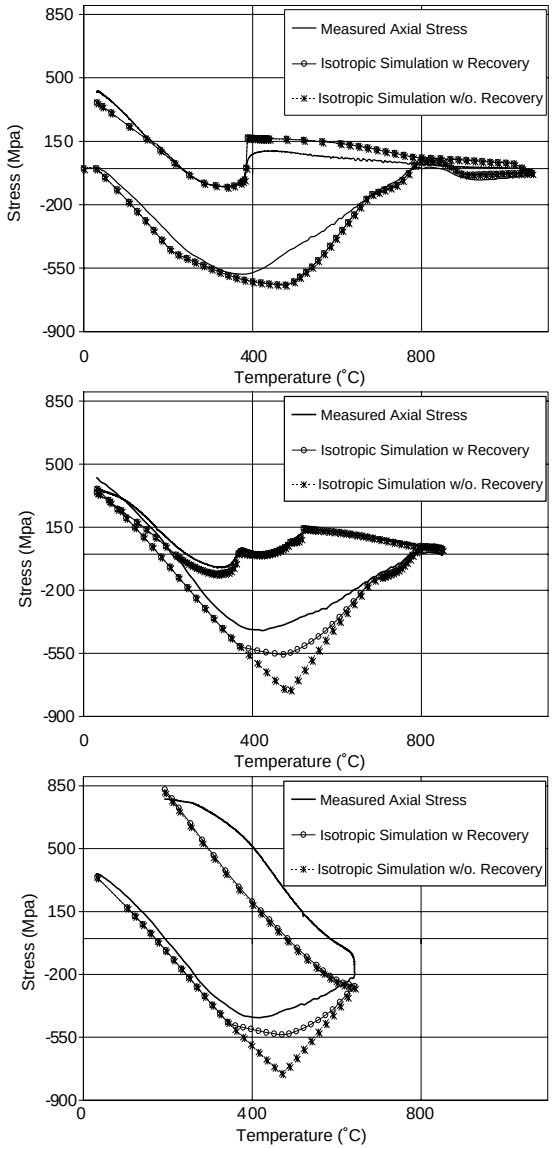

Fig. 17. Comparison between experimental results and numerical simulations with and without strain hardening recovery Satoh test 12.

the first thermal cycle, the difference in behavior occurs after the transformation during cooling has been completed, when the bainitic phase reaches the macroscopic plasticity threshold. Strain hardening is transmitted from the mother phase to the child phase through the effective internal variable E_{γ}^{eff}, which leads to an increase in the plasticity threshold by simple dilatation and an overestimation of the stress level upon return to ambient temperature, as shown by the comparative curve.

In Satoh test 12, at the end of the first two thermal cycles, the resulting stress at ambient temperature is less than the elastic limit of the monophasic or polyphasic constituent generated. Therefore, the transmission of strain hardening from the mother phase to the child phase does not modify the stress level after return to ambient temperature for the first two cycles. Its influence begins only during reheating in the last two cycles.

Up to now, few experimental works have been carried out in order to quantify this phenomenon. Is there partial or total recovery of strain hardening of the mother phase during the transformation? How is this strain hardening transmitted? Is the mixed nature of strain hardening of the mother phase preserved? It was not possible with these comparative results alone to give a definite answer. Globally, if one takes into account the transmission of strain hardening from the mother phase to the martensitic or bainitic phase, the numerical simulations yield less satisfactory results.

6. Conclusion

The objective of this study was to compare, in the case of 16MND5 steel, the prediction obtained by the models taking into account metallurgical effects which exist in the SYSWELD® code (ESI). The comparison was based on the numerical simulation of very specific tests of the "Satoh" type. These tests consist of austenitizing, then cooling homogeneously a cylindrical test piece whose longitudinal displacements in the useful zone are restrained. In this case, virtually all the thermo-mechanical and thermo-metallurgical phenomena which can be observed in the HAZ are present simultaneously. For that reason, the Satoh tests are very useful in validating the constitutive relations used to describe the mechanical evolution in the HAZ. In carrying out the Satoh tests, we considered three types of thermal loading which lead to different types of transformations during heating and cooling. Numerical simulations corresponding to these tests were performed with the finite element code SYSWELD® (ESI). The comparative analyses of the calculations and the experiments enabled us to test the kinematic and isotropic models included in the program and to analyze the sensitivity of the various significant phenomena, such as transformation-induced plasticity and strain hardening recovery.

The analysis of the experimental results showed the mixed nature of strain hardening of the phases involved and pointed out the influence of phenomena related to high-temperature viscosity. The procedure we implemented also enabled us to pinpoint the influence of the applied stress on the characteristics of the transformations. This stress activates the transformation and a significant increase in the temperatures at which phase transformations begin can be observed. The comparative analyzes showed the important role played by the transformation-induced plasticity phenomenon. However, in certain cases, regardless of whether the transformation-induced plasticity strain rate is taken into account or not, the stress at ambient temperature is more or less the same despite the very different situations of stress evolution. Therefore, one can stress the point that obtaining a correct level of residual stresses in a welding process does not guarantee that the phenomena occurring during structural transformations have been modeled correctly. During structural transformations, the two formalisms, kinematic and isotropic, produce quite different results. We showed the influence of the internal variables on the evolution of the stress. While the kinematic calculation tends to underestimate the decrease of the stress during the metallurgical transformation, the isotropic calculation overestimates it. In conclusion, a mixed isotropic and kinematic strain hardening law could represent the behavior of the steel considered more accurately, whether phase transformations

occur or not. It was not possible to derive a final conclusion on the strain hardening recovery phenomenon. Globally, if one takes into account the transmission of strain hardening from the mother phase to the martensitic phase or the bainitic phase, the numerical simulations give less satisfactory results. As a final conclusion, the comparative analyzes showed that the idea that Magee's mechanism is more significant than Greenwood and Johnson's mechanism for the martensitic transformation is questionable.

Acknowledgement

The authors wish to express their thanks to the financial support provided by Electricité de France (EDF), FRAMATOME-ANP and BCCN-DGSNR.

References

Abrassart, F., 1972. Influence des transformations martensitiques sur les propriétés mécaniques des alliages du système Fe–Ni–Cr–C, Ph.D. Thesis, Université de Nancy I.

Bergheau, J.-M., Leblond, J.-B., 1991. Coupling between heat flow, metallurgy and stress–strain computations in steels—The approach developed in the computer code SYSWELD for welding or quenching. In: Rappaz, Ozgu, Mahin (Eds.), Modeling of Casting, Welding and Advanced Solidification Processes V. The Minerals, Metals and Materials Society, pp. 203–210.

Börjesson, L., Lindgren, L.-E., 2001. Thermal, metallurgical and mechanical models for simulation of multipass welding. ASME J. Eng. Mater. Technol. 123 (Jan), 106–111.

Cavallo, N., 1998. Contribution à la validation expérimentale de modèles décrivant la ZAT lors d'une opération de soudage, Thesis, INSA, Lyon.

Cherkaoui, M., Berveiller, M., Sabar, H., 1998. Micromechanical modeling of martensitic transformation induced plasticity (TRIP) in austenitic single crystals. Int. J. Plast. 14, 597–626.

Denis, S., 1987. Influence of stresses on the kinetics of pearlitic transformation during continuous cooling. Acta Metall. 35 (7), 1621–1632.

Devaux, J., 1998. Comportement plastique des aciers en cours de transformations de phases—Etude numérique des lois de mélange et de la plasticité de transformation. Rapport Systus International LDEW98/235, p. 29.

Dupas, P., et al., 1998. Comparaison des modèles de comportement mécanique tenant compte des effets métallurgiques implantés dans le Code_Aster et Sysweld. Rapport EDF/DER HT-2C/97/070/A.

Fischer, F.D., 1997. Modelling and simulation of transformation induced plasticity in elasto-plastic materials. In: Berveiller, Fischer (Eds.), Mechanics of Solids with Phase Changes, CISM Courses and Lectures No 368. Springer Verlag, pp. 189–237.

Fischer, F.D., Reisner, G., Werner, E., Tanaka, K., Cailletaud, G., Antretter, T., 2000. A new view on transformation induced plasticity (TRIP). Int. J. Plast. 16, 723–748.

Gautier, E., 1985. Transformations perlitiques et martensitique sous contrainte de traction dans les aciers, Thèse de Doctorat ès-Sciences Physiques, Institut National Polytechnique de Lorraine, Nancy, p. 176.

Giusti, J., 1981. Contraintes et déformations résiduelles d'origine thermique—Application au soudage et à la trempe des aciers, Ph.D. thesis, Université Paris VI.

Greenwood, G.W., Johnson, R.H, 1965. The deformation of metals under small stresses during phase transformation. Proc. Roy. Soc. 283, 403–422.

Itoh, Y.Z., Kashiwaya, H., 1992. A study of cyclic thermal straining in welded joint, using a closed-loop, servo-controlled testing machine. J. Pressure Vessel Technol. Trans. ASME 114, 422–427.

Leblond, J.B., 1989. Mathematical modelling of transformation plasticity in steels II. Coupling with strain hardening phenomena. Int. J. Plast. 5, 573–591.

Leblond, J.B., 1990. Qualification expérimentale du modèle de plasticité de transformation. FRAMASOFT + CSI Internal Report n°CSS/L/NT.90/4022.

Leblond, J.B., Mottet, G., Devaux, J.C., 1986a. A theoretical and numerical approach to the plastic behaviour of steels during phase transformations I. Derivation of general relations. J. Mech. Phys. Solids 34, 395–410.

Leblond, J.B., Mottet, G., Devaux, J.C., 1986b. A theoretical and numerical approach to the plastic behaviour of steels during phase transformations II. Study of classical plasticity for ideal-plastic phases. J. Mech. Phys. Solids 34, 411–432.

Leblond, J.B., Devaux, J., Devaux, J.C., 1989. Mathematical modelling of transformation plasticity in steels I. Case of ideal-plastic phases. Int. J. Plast. 5, 551–572.

Magee, C.L, 1966. Transformation kinetics, microplasticity and ageing of martensite in Fe-3l-Ni. Ph.D. Thesis Carnegie Mellon University, Pittsburg.

Mitter, W., 1986. Umwandlungsplastizität Und Ihre Berücksichtignung Bei Der Berechnung Von Eigenspannungen. Bornträger Verlag, Asdfadsf.

Ronda, J., Oliver, G.J., 2000. Consistent thermo-mechano-metallurgical model of welded steel with unified approach to derivation of phase evolution laws and transformation-induced plasticity. Comput. Methods Apppl. Mech. Eng. 189 (2), 361–418.

Satoh, K., 1972a. Transient thermal stresses of weld heat-affected zone by both-ends-fixed bar analogy. Trans. Jpn. Weld. Soc. 3 (1), 125–134.

Satoh, K., 1972b. Thermal stresses developed in high-strength steels subjected to thermal cycles simulating weld heat-affected zone. Trans. Jpn. Weld. Soc. 3 (1), 135–142.

Simon, A., Denis, S., Gautier, E., 1994. Effet des sollicitations thermo-mécaniques sur les transformations de phases dans l'état solide. Aspects métallurgique et mécanique. Journal de Physique IV 4, 199–213 (Colloque C3 supplément au journal de physique III).

Sjöström, S., 1984. Interactions and constitutive models for the calculation of quench stresses in steel. Calculation of internal stresses in heat treatment of metallic materials. Int. Symposium, 23–24 May, Linköping, Sweden, pp. 221–246.

Taleb, L., 1998. Etude du comportement mécanique des aciers en cours de transformations métallurgiques—Synthèse des résultats des essais base de données pour les transformations uniques. Rapport INSA/URGC-Structures 1/972/005a, 17p.

Videau, J.C., Cailletaud, G., Pineau, A., 1994. Modélisation des effets mécaniques des transformations de phases pour le calcul des structures. Journal de Physique IV 4, 227–232 (Colloquium C3, extra issue to Journal de Physique III).

Vincent, Y., 2002. Simulation numérique des conséquences métallurgiques et mécaniques induites par une opération de soudage—Acier 16MND5. Thesis, INSA, Lyon.

Wang, Z.G., Inoue, T., 1985. Viscoplastic constitutive relation incorporating phase transformation—Application to welding. Mater. Sci. Technol. 1, 899–903.